

Article

Visible Measurement of Terahertz Power Based on Capsulized Cholesteric Liquid Crystal Film

Lei Wang^{1,2,*}, Hongsong Qiu², Thanh Nhat Khoa Phan², Kosaku Kato², Boyoung Kang³, Keisuke Takano², Yanqing Lu⁴, Lujian Chen⁵, Peng Lv¹, Kehan Yu¹, Wei Wei¹, Biaobing Jin⁶ and Makoto Nakajima^{2,*}

¹ College of Electronic and Optical Engineering & College of Microelectronics, Nanjing University of Posts and Telecommunications, Nanjing 210023, China; lvp@njupt.edu.cn (P.L.); kehanyu@njupt.edu.cn (K.Y.); weiwei@njupt.edu.cn (W.W.)

² Institute of Laser Engineering, Osaka University, Suita, Osaka 565-0871, Japan; qiu-hongsong@ile.osaka-u.ac.jp (H.Q.); phan@ile.osaka-u.ac.jp (T.N.K.P.); kato-ko@ile.osaka-u.ac.jp (K.K.); ksk_takano@shinshu-u.ac.jp (K.T.)

³ Center for Advanced Meta-Materials, Daejeon 305-343, Korea; bykang@kimm.re.kr

⁴ National Laboratory of Solid State Microstructures, Collaborative Innovation Center of Advanced Microstructures and College of Engineering and Applied Sciences, Nanjing University, Nanjing 210093, China; yqlu@nju.edu.cn

⁵ Department of Electronic Engineering, Xiamen University, Xiamen 361005, China; lujianchen@xmu.edu.cn

⁶ Research Institute of Superconductor Electronics (RISE), School of Electronic Science and Engineering, Nanjing University, Nanjing 210093, China; bbjin@nju.edu.cn

* Correspondence: wangl@njupt.edu.cn (L.W.); nakajima-m@ile.osaka-u.ac.jp (M.N.)

Received: 27 October 2018; Accepted: 10 December 2018; Published: 12 December 2018



Abstract: We demonstrate a new method to detect terahertz (THz) power using a temperature-supersensitive capsulized cholesteric liquid crystal film based on the thermochromic and thermodiffusion effect, which is clearly observed. A quantitative visualization of the THz intensity up to 4.0×10^3 mW/cm² is presented. The diameter of the color change area is linearly dependent on the THz radiation power above 0.07 mW in the steady state. Moreover, the THz power can be detected for 1 sec of radiation with a parabolic relation to the color change area. The THz power meter is robust, cost-effective, portable, and even flexible, and can be used in applications such as THz imaging, biological sensing, and inspection.

Keywords: terahertz; cholesteric liquid crystal; quantitative visualization

1. Introduction

Terahertz (THz) radiation in the range of 0.1–10 THz has enormous advantages such as a low photon energy, sensitivity to free carrier, crystal lattice vibration, magnetic spins, hydrogen bonds, intermolecular interaction, water, and high transparency for non-conducting materials. THz technology is, therefore, promising for a diverse range of applications from spectroscopy, security screening and biomedical technology to high-speed wireless communication [1–7]. Many types of THz sources such as photoconductive antenna, semiconductor, magnetic materials, nonlinear optical crystal, cascade laser, resonant tunneling diode, and air plasma were developed [3,8–19]. The intensity and conversion efficiency are becoming very well recently. THz wave detection plays a key role in all of these areas. Conventional THz detectors are primarily divided into noncoherent and coherent types. Noncoherent THz thermal detectors typically based on the pyroelectric or bolometric effect are widely used in THz imaging [20–22]. However, these devices detect THz radiation based on electronic measurement, which requires complex fabrication and is bulky and expensive. The Golay detector can measure THz

radiation through the optical method, but it is fragile and sensitive to mechanical vibration, has a slow response, and has too low a THz power (maximum $\sim 10 \mu\text{W}$) to be detected [23]. THz detectors still have outstanding challenges to address before becoming cost-effective, user-friendly, and widely used.

Recently, alternative thermal detection techniques using cholesteric liquid crystals (CLCs) have emerged. CLCs have the intrinsic self-organizing ability of a helical structure, the pitch of which depends on temperature, and the wavelength of the selective reflection depends on the pitch [24,25]. THz radiation increases the temperature of CLCs, which changes the pitch. Therefore, THz power is detected through measurement of the reflective wavelength. THz waves induce color change of CLCs, which can be observed directly by the naked eye, thus makes electronic devices, power supplies, or connecting cables unnecessary. This simplicity enables us to make cheap and portable THz imagers. The first CLC imager for 337- μm radiation was demonstrated by Keilmann and Renk in 1971 [26]. In 2013, Woolard et al. reported a CLC imager for THz quantum cascade lasers [27]. Both are for single-frequency THz radiation. With the rapid development of various broadband and high-power THz sources pumped by table-top lasers, we have used a temperature-sensitive CLC to measure the THz beam profile. We have measured the THz beam profiles at low power density under which condition the influence of thermodiffusion-effect CLC film can be neglected [28]. Under a high THz power density, the thermochromatic and thermodiffusion effect always exists simultaneously in the CLC. Especially, while the color does not change at the center of the CLC film at the saturation, the color change can still diffuse to a larger area in the CLC, which is stable, easy to investigate, and can be used for designing new THz devices.

Here, we present new methods for detecting THz waves in high THz intensity using a temperature-supersensitive capsulized CLC film (CCLCF). We utilize not only the thermochromic effect but also the thermal diffusion effect of the CLCs to quantify the THz absorption-induced increase in the size of the color change area. By focusing the THz beam, the power density reaches as high as $4.0 \times 10^3 \text{ mW}/\text{cm}^2$. In the equilibrium state, the diameter of the color change area is linearly related to the THz power, whereas in the transient state, for 1 sec of THz radiation, the THz power can also be clearly detected.

2. Materials and Methods

The configuration of the CCLCF is illustrated in Figure 1. It consists of three layers. The CLCs are encapsulated in droplets of $\sim 10 \mu\text{m}$ in size dispersed in an organic solvent (RM2325, Capsular Products, Tokyo, Japan), shown in the inset of Figure 1, which is directly coated on the acrylic resin layer. The carbon black layer adheres to the CCLC layer from the back side, in order to clearly change the color of the CCLCF. This thin film is flexible and pressure-insensitive, which makes it easy to scale up for operation.

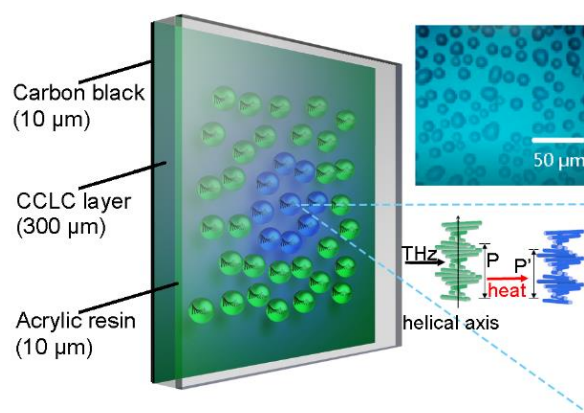


Figure 1. Schematic and working principle of the capsulized cholesteric liquid crystal film (CCLCF). The inset shows a micrograph of the CCLCF, which is produced with a color 3D laser scanning microscope (VK-8710, KEYENCE, Osaka, Japan).

We harness the heat produced by the localized absorption of the THz radiation to increase the temperature of the CCLCF. Thus, the helical pitch of the CCLC is shortened, simultaneously resulting in both a color change and increase in size. This is the process of producing an image of the color change that is dependent on the THz intensity. Especially when the THz radiation is focused, the high THz power density clearly reveals the diffusion of the color change. The THz radiation is measured by analyzing the image. The device is not restricted by the saturation of the color change and is stable and practical without any additional components required to measure the temperature.

The narrow temperature range of the color change is better for the sensitivity of the THz power measurement. Our thermochromic LC is temperature-supersensitive, which is from about 22 °C to 25.5 °C, as shown in Figure 2, at a room temperature of 23.8 °C, and green light is reflected while the color changes to blue (corresponding to the saturation) when the temperature reaches 25.5 °C, increasing by just 1.7 °C. The inset pictures were taken by a common commercial digital camera and show that the film is very homogeneous. The curves represent the THz absorptance spectra at different temperatures. The absorption $A(\omega)$ is calculated by $1 - T(\omega) - R(\omega)$, where $T(\omega)$ and $R(\omega)$ are the transmittance and reflectance of the CCLCF, respectively, measured by conventional THz time-domain spectroscopy. Compared to our earlier work [28], here we improved the sample by removing two layers Polyethylene terephthalate and double-sided tape to obtain a higher THz absorption. We can see that the THz absorption of the CCLCF is almost temperature-independent, where the absorption at 25.5 °C is a little larger than that at 23.8 °C. The THz polarization-independent characteristic is also measured and confirmed, which is not given here. The absorption increases over the entire THz region from 0 to 3 THz. The oscillation in the THz absorptance spectrum is an interference effect caused by multiple reflections of the CCLCF. The thermal conductivity of the sample we measured is about 0.5 J/msK. All the measurements indicate that the device is stable, which is suitable for our THz power detection.

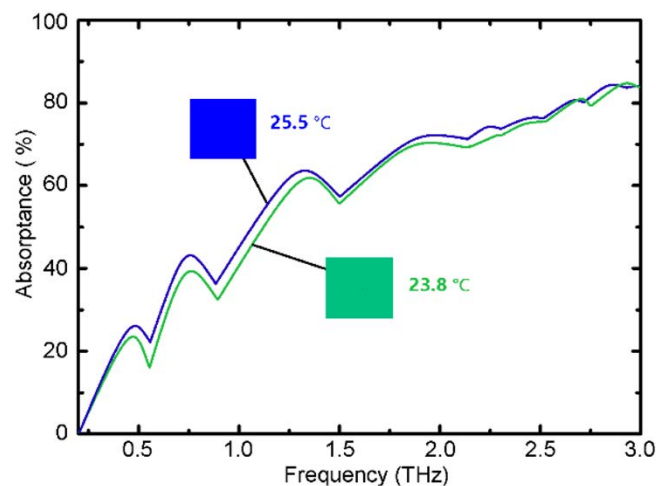


Figure 2. Effect of temperature on THz absorption spectra of CCLCF. The inset shows the photos of color change from green (23.8 °C) to blue (25.5 °C).

3. Setup and Results

Since we aim to propose a new method to detect THz power using our CLC device, the characterization of its performance in a large power range is more expected. Therefore, the THz pulse generation setup using the tilted-pump-pulse-front method [15,16], which is believed to be one of the most efficient THz sources [9,13,16], is adopted in our experiment. We generate THz pulses with pulse energy of 2.6 μ J by using pump beam with pulse energy of 4 mJ. The energy conversion efficiency is thus $\sim 0.7\%$. The advantage of our system is that the LiNbO₃ has a much higher pump-power tolerance and can generate high intensity THz waves. The much larger pump power compensates for the lack of the energy conversion efficiency. Our mW class THz source (pulse peak amplitude ~ 500 kV/cm) can be

satisfactory for many researches. The setup and the THz power measurement with the CCLCF is shown in Figure 3a. The LiNbO₃ crystal is pumped by a regeneratively amplified Ti: sapphire laser (Legend Elite: 800-nm central wavelength, 4-W optical power, 100-fs pulse duration, 1-kHz repetition rate, Coherent) to generate the broadband THz pulse. A black polypropylene filter is used to block the remaining pumped laser and the radiation produced in the crystal along with the terahertz generation. The THz source intensity is tunable by rotating the THz polarizer. The CCLCF (1.5 cm × 2.5 cm) is placed at the focal point. THz radiation is normally incident on the sample. Images and videos are taken by a smartphone camera with wireless Bluetooth technology to make it not only convenient but also to insure the detection position is fixed. The initial temperature of the CCLCF is 23.8 °C. Figure 3b shows the THz temporal profile. Single-cycle THz pulses with amplitudes of about 500 kV/cm are generated by optical rectification from LiNbO₃ [29]. Its corresponding THz spectral range is mainly 0–1 THz, which is shown in Figure 3c. The inset indicates that the THz beam spot size obtained with a THz camera (IRV-T0831, NEC, Tokyo, Japan) has a spatial profile of only about 300 μm after focusing by the parabolic mirrors. A commercial pyroelectric detector (THz-5B-MT, Gentec-EO, Quebec City, Canada) was used to calibrate and measure the THz radiation power. The maximum average THz power (P_{\max}) was 2.6 mW in our system. Thus, the maximum THz power density is as high as 4.0×10^3 mW/cm². As the focused THz beam size is very small with a high power density, the color change increases in size to a large area in the CCLCF, which can be seen clearly.

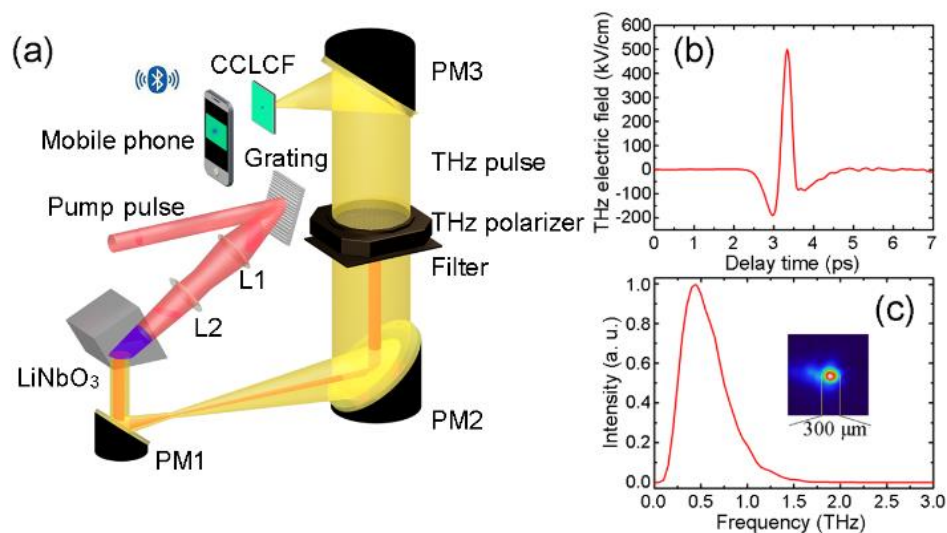


Figure 3. (a) Experimental setup. Broadband THz waves are generated by the tilted-pump-pulse-front method with a LiNbO₃ crystal. The THz beam is tightly focused into the CCLCF through off-axis parabolic mirrors (PM). (b) Measured THz temporal waveform and (c) its Fourier components. The inset shows the THz beam profile image at the focused point after PM3.

A direct visualization of different THz powers is demonstrated in Figure 4a. The images show an increase in alteration at the same area, suggesting the apparent temperature growth and thermal diffusion due to the increase in THz intensity. Without THz radiation, the green background color is a reference. Just two colors are involved, which is beneficial for our image analysis. For simple use, here we choose the diameter of the color change area as an evaluating parameter. Through the processing of our CCLCF images and videos based on hue, since hue increases monotonically with an increase in temperature [28], related parameters and data can be obtained by using software ImageJ [30]. The digital value of hue is 131. Figure 4b presents the relationship between the diameter and THz power in the steady state. The detectable THz field threshold value is about 0.07 mW, which can produce color changes visible to the naked eye. It has an approximately linear relationship above the threshold. The film still works well even when the THz intensity exceeds 4.0×10^3 mW/cm². Therefore, we quantify the THz wave intensity by the diameter of the color change of the CCLCF.

The increasing diameter looks similar to a target, which suggests an apparent temperature growth due to the increase in THz intensity. The response time is shown in Figure 4c. We can see that the CCLCF clearly has different responses with different THz powers. The entire system has corresponding images in thermodynamic equilibrium with different THz powers. With the high THz power, thermal diffusion is faster than that at low power, but the stabilization diameter is much larger, thus, the response time is slow. As can be seen, at the THz power maximum of 2.6 mW in our system, it takes about 30 sec to reach equilibrium, while at 1.3 mW, the stabilization time is about 15 sec. The images from the video captured by the camera under 2.6 mW at radiation times of 2, 5, 28, and 30 sec shown in the inset demonstrate how the diameter increases with time.

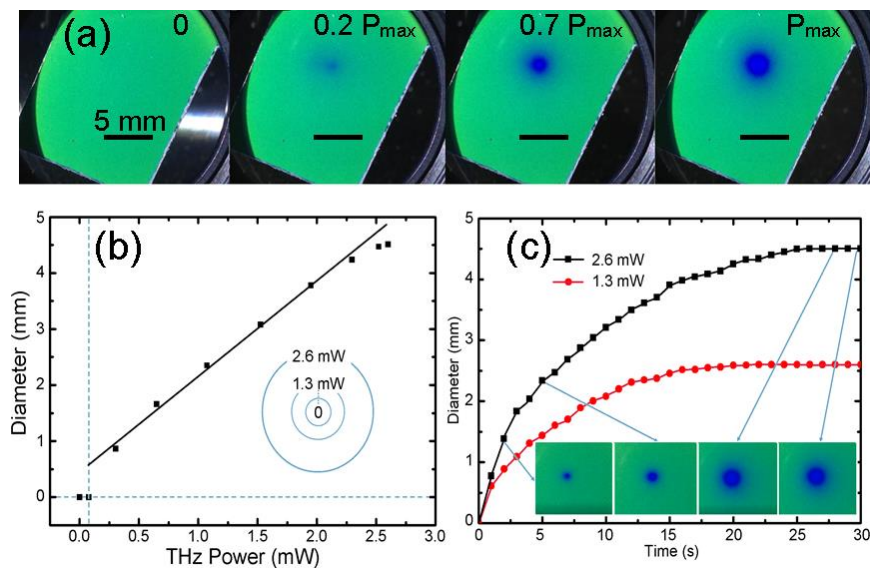


Figure 4. (a) Visible pictures are taken under different THz intensities by a smartphone camera with Bluetooth. (b) Increase in the diameter of the color change with different THz powers in thermal equilibrium, similar to the target shown in the inset. (c) Increase in the diameters as a function of response time with 1.3 and 2.6-mW THz radiation. The inset shows image changes under different THz radiation times.

For rapid THz power measurement, we switched to transient detection which means THz power can be obtained by the measurement at one point in time before the thermal equilibrium. The transient performance of the CCLCF for 1 sec of THz radiation was demonstrated in Figure 5. We varied the power by rotating the wire grid and detected the color change of the area. When the angle of the wire grid polarizer $\theta = 0^\circ$, which is parallel to the polarization of the THz wave, there is no THz transmission. Then, the angle changes to 40° , 60° , and 80° to obtain the radiation images from the video taken by the same smartphone shown in the inset. We can see that the CCLCF clearly differs for different THz powers and the response in the central small active area is more rapid than in the large active area shown in Figure 4. Here, the images are still analyzed based on hue of which the digital value we chose is 122. The THz intensity is proportional to the area of the color change. A quantitative evaluation with an approximately parabolic relation between THz power with the color change area is also obtained based on this fast measurement method.

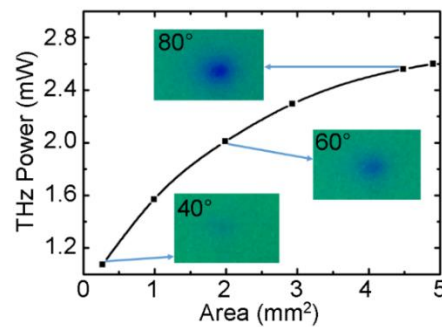


Figure 5. Relation between THz power and transient color change area when THz radiation is incident for 1 sec. The insets show the areas of color change under different THz powers.

4. Conclusions

We develop a new kind of THz power meter based on not only the thermochromic but also the thermal diffusion effect of the CCLCF, which can be used conveniently and effectively at room temperature. The THz intensity is represented as a change in color, which can be observed clearly by the naked eye and quantified through simple image analysis. Meanwhile, the radius of the THz spot is focused to only about 150 μm and the meter can measure a very high THz power density of $4.0 \times 10^3 \text{ mW}/\text{cm}^2$. Fast THz power measurement can be realized through transient detection. The performance of the THz power meter regarding sensitivity and resolution can be enhanced by improving the characteristics of the CLC, as well as image analysis methods [31,32] which may decrease the speed of the detector. There is a tradeoff we should consider. The estimated time of retrieving power after image processing should be less than one second if the whole system is completed in near future. Combined with the metamaterial [33–35], not only the amplitude of the THz wave, but also the wavelength, phase, and polarization can be detected visually in a wide frequency range, which has potential for use in practical applications.

Author Contributions: L.W. and M.N. designed the experiment. L.W., H.Q., T.N.K.P. and K.K. did the experiment. L.W., H.Q. and K.K. analyzed the experimental results. L.W., K.T., L.C. and P.L. discussed the results. L.W. wrote the paper. B.K., K.Y., W.W. and B.J. provided some valuable suggestions for the paper. Y.L. and M.N. supervised the experiment.

Funding: This research was funded by National Natural Science Foundation of China (NSFC) (61605088, 61675172); Natural Science Foundation of Jiangsu Province (BK20150845); Japan Society for the Promotion of Science (JSPS) (JP16H03886); Open Foundation Project of National Laboratory of Solid State Microstructures (M31039).

Conflicts of Interest: The authors declare no conflicts of interest.

References

1. Zhang, X.C.; Shkurinov, A.; Zhang, Y. Extreme terahertz science. *Nat. Photonics* **2017**, *11*, 16–18. [[CrossRef](#)]
2. Ferguson, B.; Zhang, X.C. Materials for terahertz science and technology. *Nat. Mater.* **2002**, *1*, 26–33. [[CrossRef](#)] [[PubMed](#)]
3. Hangyo, M. Development and future prospects of terahertz technology. *Jpn. J. Appl. Phys.* **2015**, *54*, 120101. [[CrossRef](#)]
4. Kurihara, T.; Watanabe, H.; Nakajima, M.; Karube, S.; Oto, K.; Otani, Y.; Suemoto, T. Macroscopic Magnetization Control by Symmetry Breaking of Photoinduced Spin Reorientation with Intense Terahertz Magnetic Near Field. *Phys. Rev. Lett.* **2018**, *120*, 107202. [[CrossRef](#)] [[PubMed](#)]
5. Makino, K.; Kato, K.; Takano, K.; Saito, Y.; Tominaga, J.; Nakano, T.; Isoyama, G.; Nakajima, M. Significant volume expansion as a precursor to ablation and micropattern formation in phase change material induced by intense Terahertz Pulses. *Sci. Rep.* **2018**, *8*, 2914. [[CrossRef](#)] [[PubMed](#)]
6. Wang, L.; Ge, S.; Hu, W.; Nakajima, M.; Lu, Y. Tunable reflective liquid crystal terahertz waveplates. *Opt. Mater. Express* **2017**, *7*, 2023–2029. [[CrossRef](#)]

7. Matsui, T.; Mori, H.; Inose, Y.; Kuromiya, S.; Takano, K.; Nakajima, M.; Hangyo, M. efficient optical terahertz-transmission modulation in solution-processable organic semiconductor thin films on silicon substrate. *Jpn. J. Appl. Phys.* **2016**, *55*, 03DC12. [[CrossRef](#)]
8. Burford, N.M.; El-Shenawee, M.O. Review of terahertz photoconductive antenna technology. *Opt. Eng.* **2017**, *56*, 010901. [[CrossRef](#)]
9. Berry, C.W.; Wang, N.; Hashemi, M.R.; Unlu, M.; Jarrahi, M. Significant performance enhancement in photoconductive terahertz optoelectronics by incorporating plasmonic contact electrodes. *Nat. Commun.* **2013**, *4*, 1622. [[CrossRef](#)]
10. Zhang, X.C.; Auston, D.H. Optoelectronic measurement of semiconductor surfaces and interfaces with femtosecond optics. *J. Appl. Phys.* **1992**, *71*, 326. [[CrossRef](#)]
11. Nakajima, M.; Takahashi, M.; Hangyo, M. Strong enhancement of THz radiation intensity from semi-insulating GaAs surfaces at high temperatures. *Appl. Phys. Lett.* **2002**, *81*, 1462–1464. [[CrossRef](#)]
12. Nakajima, M.; Uchida, K.; Tani, M.; Hangyo, M. Strong enhancement of terahertz radiation from semiconductor surfaces using MgO hemispherical lens coupler. *Appl. Phys. Lett.* **2004**, *85*, 191–193. [[CrossRef](#)]
13. Seifert, T.; Jaiswal, S.; Martens, U.; Hannegan, J.; Braun, L.; Maldonado, P.; Freimuth, F.; Kronenberg, A.; Henrizi, J.; Radu, I.; et al. Efficient metallic spintronic emitters of ultrabroadband terahertz radiation. *Nat. Photonics* **2016**, *10*, 483–488. [[CrossRef](#)]
14. Qiu, H.; Kato, K.; Hirota, K.; Sarukura, N.; Yoshimura, M.; Nakajima, M. Layer thickness dependence of the terahertz emission based on spin current in ferromagnetic heterostructures. *Opt. Express* **2018**, *26*, 15247–15254. [[CrossRef](#)] [[PubMed](#)]
15. Hebling, J.; Yeh, K.L.; Hoffmann, M.C.; Bartal, B.; Nelson, K.A. Generation of high-power terahertz pulses by tilted-pulse-front excitation and their application possibilities. *J. Opt. Soc. Am. B* **2008**, *25*, B6–B9. [[CrossRef](#)]
16. Hirori, H.; Doi, A.; Blanchard, F.; Tanaka, K. Single-cycle terahertz pulses with amplitudes exceeding 1 MV/cm generated by optical rectification in LiNbO₃. *Appl. Phys. Lett.* **2011**, *98*, 091106. [[CrossRef](#)]
17. Xie, X.; Dai, J.; Zhang, X.C. Coherent control of THz wave generation in ambient air. *Phys. Rev. Lett.* **2006**, *96*, 075005. [[CrossRef](#)]
18. Minami, Y.; Kurihara, T.; Yamaguchi, K.; Nakajima, M.; Suemoto, T. High-power THz wave generation in plasma induced by polarization adjusted two-color laser pulses. *Appl. Phys. Lett.* **2013**, *102*, 041105. [[CrossRef](#)]
19. Minami, Y.; Nakajima, M.; Suemoto, T. Effect of preformed plasma on terahertz-wave emission from the plasma generated by two-color laser pulses. *Phys. Rev. A* **2011**, *83*, 023828. [[CrossRef](#)]
20. NEC. THz Imager. Available online: <http://www.nec.com/en/global/prod/terahertz/> (accessed on 11 December 2018).
21. INO. IRXCAM-384 THz Terahertz Camera Module. Available online: <https://www.ino.ca/en/products/terahertz-camera-microcam-384i-thz/> (accessed on 11 December 2018).
22. Ophir Photonics. Pyrocam IIIHR Beam Profiling Camera. Available online: <http://www.ophiropt.com/laser--measurement/beam-profilers/products/Beam-Profiling/Camera-Profiling-with-BeamGage/Pyrocam-IIIHR> (accessed on 11 December 2018).
23. TYDEX. Golay Detectors. Available online: http://www.tydexoptics.com/products/thz_devices/golay_cell/ (accessed on 11 December 2018).
24. Wang, L.; Urbas, A.M.; Li, Q. Nature-Inspired Emerging Chiral Liquid Crystal Nanostructures: From Molecular Self-Assembly to DNA Mesophase and Nanocolloids. *Adv. Mater.* **2018**, e1801335. [[CrossRef](#)]
25. Schwartz, M.; Lenzi, G.; Geng, Y.; Rønne, P.B.; Ryan, P.Y.A.; Lagerwall, J.P.F. Cholesteric Liquid Crystal Shells as Enabling Material for Information-Rich Design and Architecture. *Adv. Mater.* **2018**, *30*, 1707382. [[CrossRef](#)] [[PubMed](#)]
26. Keilmann, F.; Renk, K.F. Visual observation of submillimeter wave laser beams. *Appl. Phys. Lett.* **1971**, *18*, 452. [[CrossRef](#)]
27. Chen, I.A.; Park, S.W.; Chen, G.; Wang, C.; Bethea, C.; Martini, R.; Woolard, D. Ultra-broadband wavelength conversion sensor using thermochromic liquid crystals. *Proc. SPIE* **2013**, *8624*, 862415.
28. Tadokoro, Y.; Nishikawa, T.; Kang, B.; Takano, K.; Hangyo, M.; Nakajima, M. Measurement of beam profiles by terahertz sensor card with cholesteric liquid crystals. *Opt. Lett.* **2015**, *40*, 4456–4459. [[CrossRef](#)] [[PubMed](#)]

29. Nakajima, M.; Kurihara, T.; Tadokoro, Y.; Kang, B.; Takano, K.; Yamaguchi, K.; Watanabe, H.; Oto, K.; Suemoto, T.; Hangyo, M. Application of Terahertz Field Enhancement Effect in Metal Microstructures. *J. Infrared Milli. Terahertz Waves* **2016**, *37*, 1199–1212. [[CrossRef](#)]
30. Schneider, C.A.; Rasband, W.S.; Eliceiri, K.W. NIH Image to ImageJ: 25 years of image analysis. *Nat. Methods* **2012**, *9*, 671–675. [[CrossRef](#)]
31. Goldszal, A.F.; Davatzikos, C.; Pham, D.L.; Yan, M.X.; Bryan, R.N.; Resnick, S.M. An image-processing system for qualitative and quantitative volumetric analysis of brain images. *J. Comput. Assist. Tomogr.* **1998**, *22*, 827–837. [[CrossRef](#)] [[PubMed](#)]
32. Zhou, X.; He, J.; Liao, L.S.; Lu, M.; Ding, X.M.; Hou, X.Y.; Zhang, X.M.; He, X.Q.; Lee, S.T. Real-time observation of temperature rise and thermal breakdown processes in organic LEDs using an IR imaging and analysis system. *Adv. Mater.* **2000**, *12*, 265–269. [[CrossRef](#)]
33. Kang, B.; Takano, K.; Nakajima, M.; Choi, S.B.; Kim, D.; Lee, H. Portable THz imager based on a Metamaterial-Cholesteric Liquid Crystal Hybrid Structure. In Proceedings of the 42nd International Conference on Infrared, Millimeter, and Terahertz Waves (IRMMW-THz), Cancun, Mexico, 27 August–1 September 2017.
34. Wang, L.; Ge, S.; Hu, W.; Nakajima, M.; Lu, Y. Graphene-assisted high-efficiency liquid crystal tunable terahertz metamaterial absorber. *Opt. Express* **2017**, *25*, 23873–23879. [[CrossRef](#)] [[PubMed](#)]
35. Kurihara, T.; Nakamura, K.; Yamaguchi, K.; Sekine, Y.; Saito, Y.; Nakajima, M.; Oto, K.; Watanabe, H.; Suemoto, T. Enhanced spin-precession dynamics in a spin-metamaterial coupled resonator observed in terahertz time-domain measurements. *Phys. Rev. B* **2014**, *90*, 144408. [[CrossRef](#)]



© 2018 by the authors. Licensee MDPI, Basel, Switzerland. This article is an open access article distributed under the terms and conditions of the Creative Commons Attribution (CC BY) license (<http://creativecommons.org/licenses/by/4.0/>).